IEEE Access
Multidisciplinary | Rapid Review | Open Access Journal

Received October 5, 2019, accepted October 30, 2019, date of publication November 12, 2019, date of current version November 21, 2019.

Digital Object Identifier 10.1109/ACCESS.2019.2953141

Asymmetrical Multi-Step Direct Model Predictive Control of Nine-Switch Inverter for Dual-Output Mode Operation

OZAN GULBUDAK, (Member, IEEE), AND MUSTAFA GOKDAG
Department of Electrical and Electronics Engineering, College of Engineering, Karabuk University, 78050 Karabuk, Turkey

Corresponding author: Ozan Gulbudak (ozangulbudak@karabuk.edu.tr)

This work was supported by The Scientific and Technological Research Council of Turkey (TUBITAK) under Grant 117E769.

ABSTRACT Nine-Switch Inverter (NSI) is composed of two conventional inverters with three common switches. Two sets of three phase ac loads can be connected to the outputs of NSI and independently controlled without any undesirable interaction. In conventional multi-step Model Predictive Control (MPC) of a nine-switch inverter, the prediction steps of both load stages must be equal. Unfortunately, this results in losing the freedom of selecting independent prediction horizon for individual loads. To overcome this problem, a novel asymmetrical multi-step direct model predictive control method is presented in this paper. The proposed method finds two independent optimum solutions for each load to match with their utilization profile. It is assumed that two individual loads are controlled by two separate virtual inverters, and two separate model predictive control problems with their own prediction steps are solved to identify optimum control actions. The control calculations are performed in a Cyclone IV Field Programmable Gate Array (FPGA) by using a pipelined architecture. The system stability is analyzed using Lyapunov stability method. To highlight the effectiveness of introduced strategy, mathematical proof for controlling two separate loads with an asymmetrical prediction step is validated in experimentally.

INDEX TERMS Model predictive control, nine-switch inverter, FPGA, digital control, dual-output inverter systems.

I. INTRODUCTION

Voltage Source Inverters (VSIs) are the most common dc-ac power converters employed in any power conversion systems. The well-known 2-level VSI can be applied to wide range of applications, such as medium or high power traction systems and industrial drives. For the case of distributed loads, multiple VSIs need to be used to control separate ac loads. Even though using separate VSI for each individual load provides reliable operation, it increases the system complexity and volume. In this regard, nine-switch inverter, see Fig. 1, has been proposed to control multiple ac loads using a less number of semiconductors. Conceptually, NSI has come out by merging of two voltage source inverters together and it has six independent output terminals. This new topology is gaining attention due to its advantages over traditional parallel inverter system (see Fig.2) in terms of size, cost and weight. NSI-based systems have been used in wide range of energy conversion systems. In [1]–[4], uninterruptible power supplies (UPS) and power conditioners interfacing with the utility grid have been presented. In [5], bidirectional Z-Source nine-switch inverter has been used for providing clean power to electrical cars. The other interesting application has been presented in [6] to control symmetrical six-phase induction machine fed by a nine-switch inverter.

The increasing computational power in digital control platforms facilitates the applications of model predictive control to power converters. MPC is ubiquitous in industrial applications, as it enables the control of strongly nonlinear systems with constraints, which are difficult to handle using traditional linear controller. MPC benefits from intuitive tuning and the ability to control a range of simple and complex systems including with dynamic constraints [7]–[10]. In addition, it is straightforward to incorporate known control constraints and multiple operating conditions, and it provides the flexibility to formulate a cost function. MPC and its enhancements have been successfully implemented in a large variety of power electronics applications [11]–[15].

The associate editor coordinating the review of this manuscript and approving it for publication was Bohui Wang.

This work is licensed under a Creative Commons Attribution 4.0 License. For more information, see http://creativecommons.org/licenses/by/4.0/

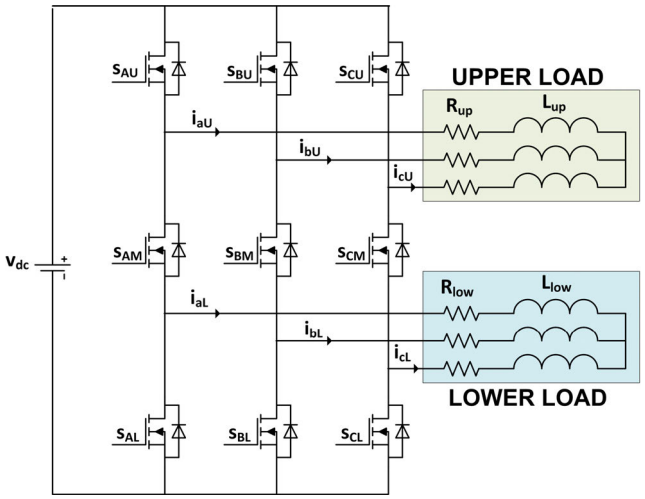

FIGURE 1. Nine-Switch Inverter (NSI) based multi drive system.

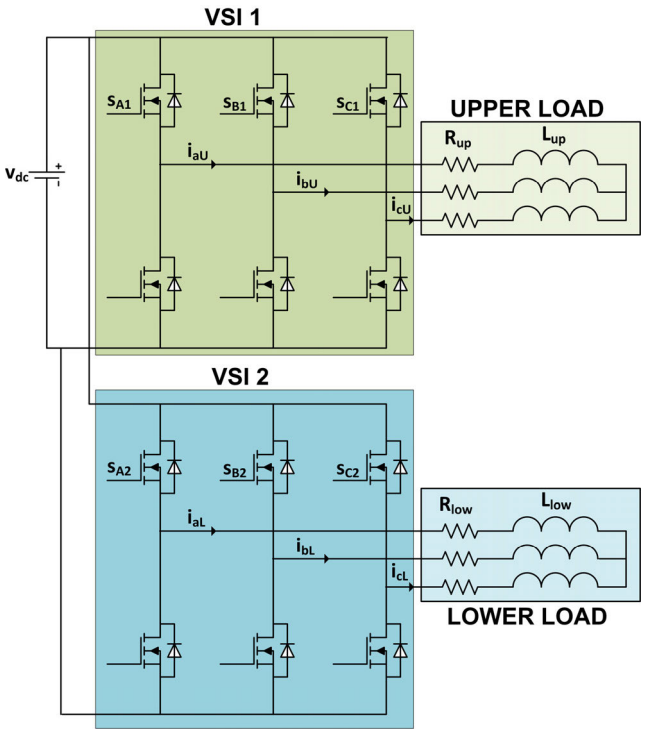

FIGURE 2. Traditional voltage source inverter based multi-drive system.

Despite the great success and rapid development of MPC, there are several challenges limiting the applicability to power converter control problems. The major drawback of model predictive control method in power electronics is high computational burden since corresponding objective function needs to be solved for each possible control actuation. In literature, several different approaches have been presented to handle this high computational demand [16]–[19]. Among these methods, an FPGA-based model predictive control approach is more promising solution due to its flexibility. The main idea of an FPGA-based MPC is that required control calculations can be paralleled in different areas of an FPGA and the execution time can be significantly reduced. Since MPC has many independent repeated operations, processing can be evenly divided into uniform latency sub-operations.

In conventional MPC of nine-switch inverter, single multi objective cost function is evaluated for all allowable switching combinations of NSI. The load current error terms of both load stages are introduced in the cost function and the switching state that minimizes the cost function is selected as an optimum input. For the case of multi-step MPC, a prediction step (e.g. N = 1, 2 or 3) is selected for whole MPC problem and there is no chance to decouple the control of different load stages. This means that independent control of separate loads is degraded and same prediction step must be used for controlling different load stages. In order to rectify this undesirable situation, an asymmetrical multi-step MPC method is proposed in this paper. By decoupling the MPC problems of individual loads, two separate MPC problems with custom prediction steps are formulated for each load stages. Then, two different optimum input sequences, one is for upper load stage and the other one is for lower load stage, are determined and they are sequentially applied to the nine-switch inverter. This can be implemented by assuming that each load is controlled by a virtual voltage source inverter and unconnected MPC problems of separate loads are solved using associated voltage vectors of virtual voltage source inverters.

The main contribution of this paper is to present a novel asymmetrical multi-step model predictive control to achieve complete independent control of two separate ac loads using nine-switch inverter. The proposed control method provides the flexibility to employ MPC with different prediction step for each load stages. Furthermore, the control goals are decoupled and separate optimum control sequences are determined by solving two unconnected MPC problems. Furthermore, a novel switching state elimination technique is presented for optimization of multi-step MPC.

The outline of the paper is as follows: Section II describes the conventional model predictive control method of nine-switch inverter and the system model. Section III describes the proposed asymmetrical multi-step MPC technique for independent load control. Section IV presents the experimental results and Section V is the conclusion part of the paper.

II. CONVENTIONAL MODEL PREDICTIVE CONTROL OF NINE-SWITCH INVERTER

Nearly all industrial applications of model predictive control rely on empirical model of the systems. The increasing plant complexity and tighter performance specifications require models with higher accuracy. For these reasons, to obtain an accurate system model is critical in model predictive control approach.

A. NINE-SWITCH INVERTER MODEL

The nine-switch inverter circuit diagram is shown in Fig.1. The switches SAM, SBM and SCM are shared with the upper inverter stage and the lower inverter stage. As can be

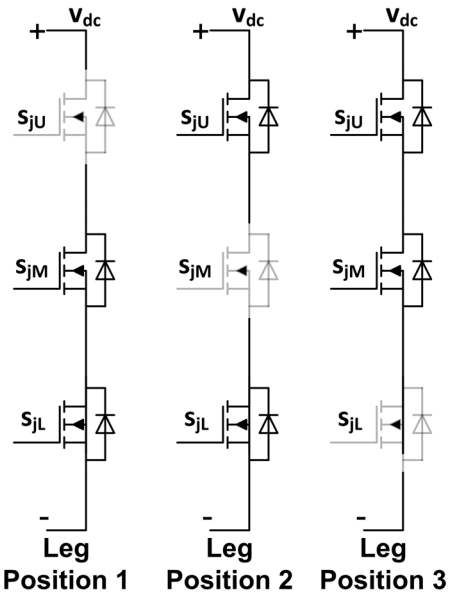

FIGURE 3. Allowable switching combinations of Nine-Switch Inverter for each leg with $j\epsilon\{A, B, C\}$.

seen from Fig. 1, each leg of NSI has three switches. For reliable converter operation, two switching restrictions must be considered. The first switching restriction is that switches on the same leg cannot be turned on at the same time. This protects the NSI against dc-bus short circuit. The second switching restriction is that at least two switches on the same leg should be on. Thus, a floating of connected inductive load is avoided. Accordingly, each leg can be in three different switch positions which are depicted in Fig. 3.

With discussed switching restrictions, nine-switch inverter has 27 different switching combinations. To express the relationship between different quantities in the system, the instantaneous transfer matrix of upper load and the instantaneous transfer matrix of lower are defined in (1) and (2) respectively.

$$\mathbf{T_U} = \begin{bmatrix} S_{AU} & S_{BU} & S_{CU} \end{bmatrix} \tag{1}$$

$$\mathbf{T_L} = \begin{bmatrix} (1 - S_{AL}) & (1 - S_{BL}) & (1 - S_{CL}) \end{bmatrix} \tag{2}$$

The relationship between inverter leg voltages and dc-link voltage for upper load stage and lower load stage are defined in (3) and (4).

$$\mathbf{V_U} = V_{DC}\mathbf{T_U^T} \tag{3}$$

$$\mathbf{V_L} = V_{DC}\mathbf{T_L^T} \tag{4}$$

where $\mathbf{V_U} = \begin{bmatrix} V_{aU} & V_{BU} & V_{cU} \end{bmatrix}^T$, $\mathbf{V_L} = \begin{bmatrix} V_{aL} & V_{bL} & V_{cL} \end{bmatrix}^T$.

B. CONVENTIONAL PREDICTIVE CONTROL SCHEME

MPC provides a robust architecture for explicitly incorporating constraints in control laws. This is of growing importance in many power electronics applications where rapid technological progress has created increased demand for control laws. The MPC is usually formulated in discrete-time domain by converting the control variables to sampled data. A system model is used to predict future behavior of control goals and a tailored objective function is evaluated for each possible control actuation. The process of taking new measurements, predicting future behavior of control goals and minimizing the cost function is repeated during each sampling interval. This whole process is called receding horizon strategy. The receding horizon strategy of MPC enables the incorporation of the constraints by enforcing the constraints on future inputs, outputs and state variables. MPC makes use of a dynamic system model to predict future outputs of the system for the prediction horizon N given the future control inputs. The control inputs are determined so that the user defined cost function is minimized. After an optimum control input is determined, control actuations are directly applied to the system without using any complicated modulator. This is why aforementioned control strategy is called direct model predictive control. For modeling the predictive controller, model of the system needs to be analyzed. In this work, two sets of three phase RL (resistive-inductive) loads are connected to the NSI. The dynamic model of the load is defined in (5).

$$v_o(t) = i_o(t)R + L\frac{di_o(t)}{dt} \tag{5}$$

In (5), R is the load resistance and L is the load inductance. In order to obtain discrete-time model of the load, the derivative term of the load model is sampled using forward Euler method:

$$\left.\frac{dx(t)}{dt}\right|_{t=k} \approx \frac{x(k+1) - x(k)}{Ts} \tag{6}$$

Ts is the sampling period for discretization process. By using (5) and (6), the discrete time model of the load is obtained in (7).

$$i_o(k+1) = i_o(k)\left[1 - \frac{RTs}{L}\right] + \frac{Ts}{L}v_o(k) \tag{7}$$

The discrete state-space model of the system is given by

$$\begin{aligned} \mathbf{x}(k+1) &= \mathbf{A}x(k) + \mathbf{B}u(k) \\ \mathbf{y}(k+1) &= \mathbf{C}\mathbf{x}(k+1) \end{aligned} \tag{8}$$

where

$$\mathbf{x}(k) = [\, i_{oaU}(k)\ i_{obU}(k)\ i_{ocU}(k)\ i_{oaL}(k)\ i_{obL}(k)\ i_{ocL}(k)\,]^T,$$

$$\mathbf{u}(k) = \begin{bmatrix} S_{AU} & S_{BU} & S_{CU} & S_{AM} & S_{BM} & S_{CM} & S_{AL} & S_{BL} & S_{CL} \end{bmatrix}^T$$

with $S_{j\alpha} \in U = \{1\ 0\}$ denoting the switch position in the phase $j \in \{A\ B\ C\}$ and $\alpha \in \{U\ L\}$, matrix $\mathbf{C} = \mathbf{I}_{6\times6}$,

$$\mathbf{A}_{6\times6} = (1 - \frac{RT_s}{L})\mathbf{I}_{6\times6},$$

$$\mathbf{B} = \begin{bmatrix} Q_{3\times3} & 0_{3\times3} & 0_{3\times3} \\ 0_{3\times3} & 0_{3\times3} & W_{3\times3} \end{bmatrix}_{6\times9}$$

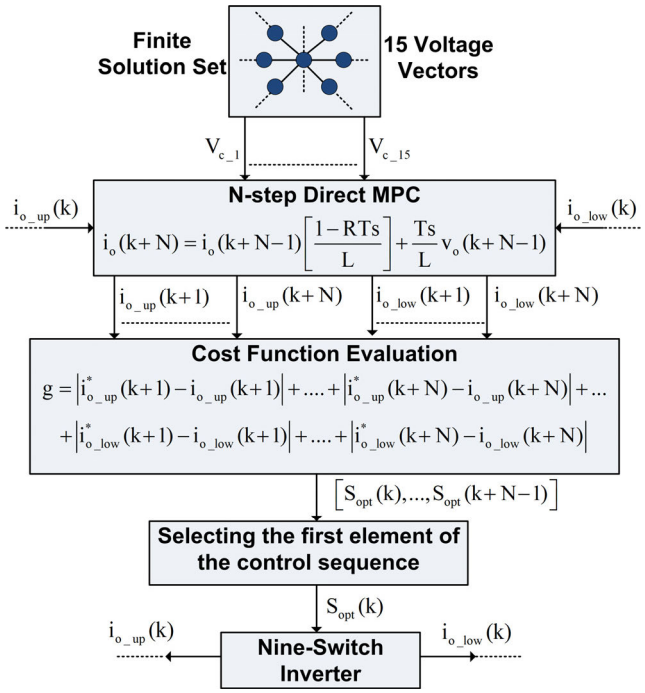

FIGURE 4. The conventional N-step direct model predictive control scheme of nine-switch inverter.

with

$$\mathbf{Q}_{3\times3} := \begin{bmatrix} \frac{2}{3} & -\frac{1}{3} & -\frac{1}{3} \\ -\frac{1}{3} & \frac{2}{3} & -\frac{1}{3} \\ -\frac{1}{3} & -\frac{1}{3} & \frac{2}{3} \end{bmatrix}_{3\times3}$$

and

$$\mathbf{W}_{3\times3} := \begin{bmatrix} -\frac{2}{3} & \frac{1}{3} & \frac{1}{3} \\ \frac{1}{3} & -\frac{2}{3} & \frac{1}{3} \\ \frac{1}{3} & \frac{1}{3} & -\frac{2}{3} \end{bmatrix}_{3\times3}.$$

In (8), $\mathbf{x}$ is the state vector which contains the control variables and $\mathbf{u}$ represents the switching positions. $\mathbf{I}_{6\times6}$ denotes the 6×6 identity matrix and $\mathbf{0}_{3\times3}$ denotes the 3×3 zero matrix. The output vector $\mathbf{y(k+1)}$ is forced to track the reference output vector $\mathbf{y^*(k+1)}$ by minimizing the objective function. The general expression for the prediction model over N-step prediction horizon can be derived by applying the state equations over the certain prediction horizon. The general expressions of state vector and output vector are defined in (9) and (10).

$$\mathbf{x}(k+N) = \mathbf{A}^N\mathbf{x}(k)+\mathbf{A}^{N-1}\mathbf{B}\mathbf{u}(k)+\ldots+\mathbf{u}(k+N-1) \quad (9)$$

$$\mathbf{y}(k+N) = \mathbf{C}\left[\mathbf{A}^N\mathbf{x}(k)+\mathbf{A}^{N-1}\mathbf{B}\mathbf{u}(k)+\ldots+\mathbf{u}(k+N-1)\right] \quad (10)$$

where, $N = 1, 2, 3, \ldots, N_H$. The input sequence over predefined horizon can be expressed as

$$\mathbf{U} = \begin{bmatrix} S_{AU}(k) & S_{AU}(k+1) & \ldots & S_{AU}(k+N-1) \\ S_{BU}(k) & S_{BU}(k+1) & \ldots & S_{BU}(k+N-1) \\ S_{CU}(k) & S_{CU}(k+1) & \ldots & S_{CU}(k+N-1) \\ \vdots & \vdots & \ddots & \vdots \\ S_{AL}(k) & S_{AL}(k+1) & \ldots & S_{AL}(k+N-1) \\ S_{BL}(k) & S_{BL}(k+1) & \ldots & S_{BL}(k+N-1) \\ S_{CL}(k) & S_{CL}(k+1) & \ldots & S_{CL}(k+N-1) \end{bmatrix}_{9\times N-1}$$
$$= \left[\mathbf{u}(k)\ \mathbf{u}(k+1)\ \ldots\ \mathbf{u}(k+N-1)\right]_{9\times N-1} \quad (11)$$

The output of state variables, which are the output load currents, are described as

$$\mathbf{Y} = \left[\mathbf{y}(k+1) \quad \mathbf{y}(k+2) \quad \ldots \quad \mathbf{y}(k+N)\right]^T \quad (12)$$

Using (8), (11) and (12), the matrix notation of whole prediction model is defined in (13).

$$\mathbf{Y}(k) = \begin{bmatrix} \mathbf{CA} \\ \mathbf{CA}^2 \\ \mathbf{CA}^3 \\ \vdots \\ \mathbf{CA}^N \end{bmatrix} \mathbf{x}(k) + \begin{bmatrix} \mathbf{CB} & 0 & 0 & \ldots & 0 \\ \mathbf{CAB} & \mathbf{CB} & 0 & \cdots & 0 \\ \mathbf{CA}^2\mathbf{B} & \mathbf{CAB} & \mathbf{CB} & \cdots & 0 \\ \vdots & \vdots & \vdots & \ddots & \vdots \\ \mathbf{CA}^{N-1} & \mathbf{CA}^{N-2}\mathbf{B} & \mathbf{CA}^{N-3}\mathbf{B} & \ldots & \mathbf{CA}^0\mathbf{B} \end{bmatrix} \mathbf{U}(k) \quad (13)$$

Over N-step prediction horizon, the reference vector is written as

$$\mathbf{Y}^*(k) = \left[\mathbf{y}^*(k+1)\ \ \mathbf{y}^*(k+2)\ \ \ldots\ \ \mathbf{y}^*(k+N)\right]^T \quad (14)$$

As a final step of the direct model predictive controller design, a proper objective function needs to be defined to compensate the load current errors for both load stages. The cost function for load current control is defined as

$$g = \sum_{\lambda=1}^{N} \left|y^*(k+\lambda) - y(k+\lambda)\right| \quad (15)$$

where k is the sampling parameter. The main goal of designed predictive controller tries to keep the error vectors as small as possible. In this design, no weighting factor is used to tune system performance. Since both error terms are in the same nature, independent load current control is achieved without using weighting factors.

During the process of minimizing the objective function, only 15 voltage vectors are used. NSI has 27 switching combinations, but some of them redundant. For that reason, 15 among 27 vectors are enough to search an optimum input. This reduction significantly reduces computational burden during the online optimization process. In Fig. 4, the main

principle of conventional N-step direct model predictive control strategy of nine-switch inverter is presented. The first step is to predict the upper load current and the lower load current over N prediction horizon. Then, these predictions and all required extrapolated references are used to evaluate the objective function. The optimum input sequence that minimizes the objective function is selected and the first element of optimum input sequence is applied to the system for the next time interval. As can be seen from Fig. 4, the prediction horizon is fixed for upper load control problem and lower load control problem. As a result, the conventional multi-step direct MPC approach does not offer a flexibility of choosing independent prediction horizon for different load stages.

C. STABILITY ANALYSIS OF THE SYSTEM

In Finite Control Set Model Predictive Control (FCS-MPC) methods, the practical Lyapunov stability criterion has been used to explore stability characteristics of the systems [20]–[23]. These approaches usually provide insights on how an error exists in the system decays to zero or negligible value after a certain amount sampling cycles are passed through. The switching function vectors of upper load stage and lower load stages are presented in (16) and (17).

$$\mathbf{S}_{\text{up}} = \frac{2}{3}(\mathrm{S_{AU}} + \mathrm{aS_{BU}} + \mathrm{a^2 S_{CU}}) \tag{16}$$

$$\mathbf{S}_{\text{low}} = \frac{2}{3}((1-\mathrm{S_{AL}}) + \mathrm{a}(1-\mathrm{S_{BL}}) + \mathrm{a^2}(1-\mathrm{S_{CL}})) \tag{17}$$

where $\mathrm{a} = \mathrm{e}^{j2\pi/3}$ is a unitary vector, which represents the 120^0 phase displacement between the phases. For representing the switching function vectors, the state space notation is used. Using (16) and (17), the output voltage vectors are defined as

$$\begin{aligned}\mathbf{V}_{\mathrm{oU}} &= V_{DC}\mathbf{S}_{\text{up}} - \mathrm{V_{nN\_up}}\frac{2}{3}(1+\mathbf{a}+\mathbf{a}^2)\\ &= \frac{2}{3}(\mathrm{V_{oaU}} + \mathbf{a}\mathrm{V_{obU}} + \mathbf{a}^2\mathrm{V_{ocU}})\end{aligned} \tag{18}$$

$$\begin{aligned}\mathbf{V}_{\mathrm{oL}} &= \mathrm{V_{DC}}\mathbf{S}_{\text{low}} - \mathrm{V_{nN\_low}}\frac{2}{3}(1+\mathbf{a}+\mathbf{a}^2)\\ &= \frac{2}{3}(\mathrm{V_{oaL}} + \mathbf{a}\mathrm{V_{obL}} + \mathbf{a}^2\mathrm{V_{ocL}})\end{aligned} \tag{19}$$

where $\mathrm{V_{nN\_up}}$ and $\mathrm{V_{nN\_low}}$ represent the common mode voltage for corresponding load stages. The output voltage vectors with unavoidable quantization errors are given below:

$$\mathrm{V}^{\approx}_{\mathrm{oU}}(\mathrm{k}) = \mathrm{V_{oU}}(\mathrm{k}) + \phi_{\mathrm{U}}(\mathrm{k}) \tag{20}$$

$$\mathrm{V}^{\approx}_{\mathrm{oL}}(\mathrm{k}) = \mathrm{V_{oL}}(\mathrm{k}) + \phi_{\mathrm{L}}(\mathrm{k}) \tag{21}$$

where $\phi_\alpha(\mathrm{k})$ are the quantization errors with $\alpha \in \{U\ L\}$ and satisfy the condition of $\phi_\alpha(\mathrm{k}) \leq \psi$ with $\psi \in \Re^+$. In (20) and (21), quantization errors are bounded since a finite number of candidate solutions are involved in control process. It can be seen from control scheme in Fig. 4 that 15 different voltage vectors are used to calculate future values of control variables. This definitely keeps the output voltages within certain bounds. The total current error term of the system, which the total error term of control variables, is defined as

$$\mathbf{i}_{\mathrm{o\_err}}(\mathrm{k}+1) = \mathbf{i}_{\mathrm{oU\_err}}(\mathrm{k}+1) + \mathbf{i}_{\mathrm{oL\_err}}(\mathrm{k}+1) \tag{22}$$

where

$$\mathbf{i}_{\mathrm{oU\_err}}(\mathrm{k}+1) = \frac{\mathrm{Ts}}{\mathrm{L}}\mathrm{V}^{\approx}_{\mathrm{oU}}(\mathrm{k}) + \mathbf{i}_{\mathrm{oU}}(\mathrm{k})\left(1-\frac{\mathrm{RTs}}{\mathrm{L}}\right) - \mathbf{i}^*_{\mathrm{oU}}(\mathrm{k}+1) \tag{23}$$

$$\mathbf{i}_{\mathrm{oL\_err}}(k+1) = \frac{\mathrm{Ts}}{\mathrm{L}}\mathrm{V}^{\approx}_{\mathrm{oL}}(\mathrm{k}) + \mathbf{i}_{\mathrm{oL}}(\mathrm{k})\left(1-\frac{\mathrm{RTs}}{\mathrm{L}}\right) - \mathbf{i}^*_{\mathrm{oL}}(\mathrm{k}+1) \tag{24}$$

with $\mathbf{i}_{\mathrm{oU}} = \begin{bmatrix}\mathrm{i_{oaU}}\ \mathrm{i_{obU}}\ \mathrm{i_{ocU}}\end{bmatrix}^{\mathrm{T}}$ and $\mathbf{i}_{\mathrm{oL}} = \begin{bmatrix}\mathrm{i_{oaL}}\ \mathrm{i_{obL}}\ \mathrm{i_{ocL}}\end{bmatrix}^{\mathrm{T}}$. In (23) and (24), superscript "$*$" denotes the reference values. For stability analysis, it is mandatory to find a function such that current tracking error term $\mathbf{i}_{\mathrm{o\_err}}(\mathrm{k}+1)$ asymptotically converges to zero. The discrete Lyapunov function of total current error term is expressed as

$$\mathrm{L}\left[\mathrm{i_{o\_err}}(\mathrm{k})\right] = \frac{1}{2}\mathrm{i}^{\mathrm{T}}_{\mathrm{o\_err}}(\mathrm{k})\mathrm{i_{o\_err}}(\mathrm{k}) \tag{25}$$

Using (22) and (25), the rate of change of Lyapunov function can be obtained as

$$\begin{aligned}&\Delta\mathrm{L}\left[\mathrm{i_{o\_err}}(\mathrm{k})\right]\\ &= \frac{1}{2}\mathrm{i}^{\mathrm{T}}_{\mathrm{oU\_err}}(\mathrm{k}+1)\mathrm{i_{oU\_err}}(\mathrm{k}+1) - \frac{1}{2}\mathrm{i}^{\mathrm{T}}_{\mathrm{oU\_err}}(\mathrm{k})\mathrm{i_{oU\_err}}(\mathrm{k})\\ &\quad+\frac{1}{2}\mathrm{i}^{\mathrm{T}}_{\mathrm{oU\_err}}(\mathrm{k}+1)\mathrm{i_{oL\_err}}(\mathrm{k}+1) - \frac{1}{2}\mathrm{i}^{\mathrm{T}}_{\mathrm{oU\_err}}(\mathrm{k})\mathrm{i_{oL\_err}}(\mathrm{k})\\ &\quad+\frac{1}{2}\mathrm{i}^{\mathrm{T}}_{\mathrm{oL\_err}}(\mathrm{k}+1)\mathrm{i_{oU\_err}}(\mathrm{k}+1) - \frac{1}{2}\mathrm{i}^{\mathrm{T}}_{\mathrm{oL\_err}}(\mathrm{k})\mathrm{i_{oU\_err}}(\mathrm{k})\\ &\quad+\frac{1}{2}\mathrm{i}^{\mathrm{T}}_{\mathrm{oL\_err}}(\mathrm{k}+1)\mathrm{i_{oL\_err}}(\mathrm{k}+1) - \frac{1}{2}\mathrm{i}^{\mathrm{T}}_{\mathrm{oL\_err}}(\mathrm{k})\mathrm{i_{oL\_err}}(\mathrm{k})\end{aligned} \tag{26}$$

According to direct Lyapunov stability method, the solution of the system prediction model (7) is practically stable if Lyapunov function $\Delta\mathrm{L}\left[\mathrm{i_{o\_err}}\right]$ is always negative. To satisfy this condition, the following inequalities (27) can be used to determine the stability properties of a function $\mathrm{L}[F(\mathrm{k})]$ with $\mathrm{L}: \Re^{\mathrm{N}} \rightarrow \Re_{\geq 0}$ [20].

$$\begin{aligned}\mathrm{L}[\mathrm{F(k)}] &\geq \mathrm{c_1}\,|\mathrm{F(k)}|^{\sigma}, \quad \forall \mathrm{F(k)} \in \mathrm{G}\\ \mathrm{L}[\mathrm{F(k)}] &\leq \mathrm{c_2}\,|\mathrm{F(k)}|^{\sigma}, \quad \forall \mathrm{F(k)} \in \Gamma\\ L[\mathrm{F(k+1)}] &- |\mathrm{F(k)}| < -\mathrm{c_3}\,|\mathrm{F(k)}|^{\sigma} + \mathrm{c_4}\end{aligned} \tag{27}$$

where $\mathrm{c_1}, \mathrm{c_2}, \mathrm{c_3}$ and $\mathrm{c_4}$ are the positive constants. The parameter σ must be equal to or greater than 1. $\mathrm{G} \subseteq \mathrm{R^N}$ is a control set and $\Gamma \subseteq \mathrm{G}$ is a compact set. If $\mathrm{G} \triangleq \Re^{\mathrm{N}}$ then, the function L is said to be practical Lyapunov function in G. The stability condition (27) is satisfied by the constant values as

$$\begin{aligned}\mathrm{c_1} &= \mathrm{c_2} = 1\\ \mathrm{c_3} &= \frac{1}{2}\\ \mathrm{c_4} &= \frac{1}{2}\left(\frac{\mathrm{Ts}}{\mathrm{L}}\right)^2(\phi_{\mathrm{U}} + \phi_{\mathrm{L}})^2\end{aligned} \tag{28}$$

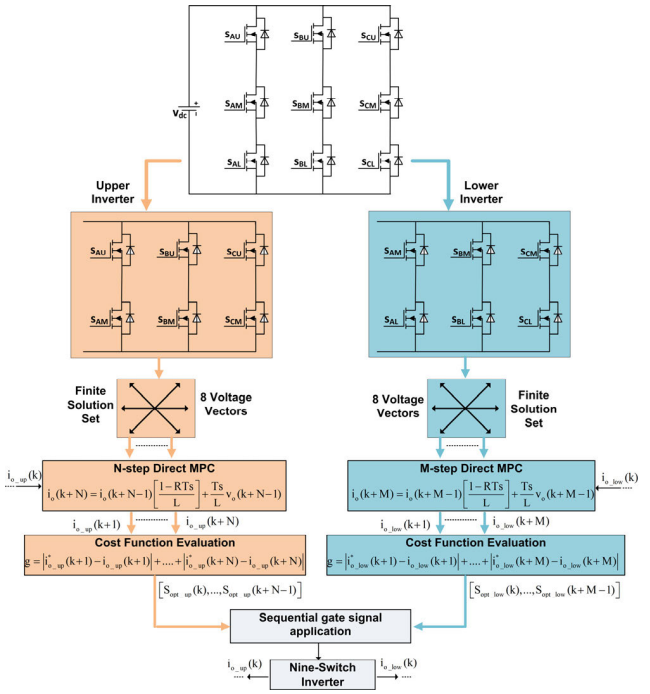

FIGURE 5. Proposed asymmetrical multi-step direct model predictive control scheme.

where,

$$F(k) = i^{T}_{oU\_err}(k)i_{oU\_err}(k) + i^{T}_{oU\_err}(k)i_{oL\_err}(k) + i^{T}_{oL\_err}(k)i_{oU\_err}(k) + i^{T}_{oL\_err}(k)i_{oL\_err}(k) \quad (29)$$

III. PROPOSED DIRECT MODEL PREDICTIVE CONTROL STRATEGY OF NINE-SWITCH INVERTER

In proposed method, the model predictive control problems of upper load stage and lower load stage are divided into two parts so as to achieve a flexibility of selecting independent prediction horizon. The essential idea behind the proposed technique is depicted in Fig. 5. Each load is assumed to be controlled by a voltage source inverter and an optimum control actuation can be identified by performing a detached MPC algorithm. After two uncoupled optimal input vectors are determined, the first elements of each input vectors are sequentially applied to nine-switch inverter.

A. PREDICTION MODEL

When abrupt changes occur in the system, an effective controller must rapidly characterize and compensate for the new dynamics. To be able to effectively control a system using MPC, a precise prediction model is necessary to calculate future values of control goals. Since each load is assumed to be controlled by a voltage source inverter, a proper prediction model needs to be derived according to voltage source inverter system. In this section, the prediction model will be given only for upper load stage. Using same approach, required prediction model can be also derived for lower load stage. The state-space model of upper inverter stage connected to RL load is defined in (30).

$$\mathbf{x_{UP}}(k+1) = \mathbf{A_{UP}x_{UP}}(k) + \mathbf{Qu_{UP}}(k)$$
$$\mathbf{y_{UP}}(k+1) = \mathbf{C_{UP}x_{UP}}(k+1) \quad (30)$$

where $\mathbf{x_{UP}} = \left[\, i_{oaU}(k)\ i_{obU}(k)\ i_{ocU}(k) \,\right]^{T}$, $\mathbf{u_{UP}}(k) = \left[\, S_{AU}\ S_{BU}\ S_{CU} \,\right]^{T}$ with $S_{jU} \in U = \{1\ 0\}$ denoting the switch position in the phase $j \in \{A\ B\ C\}$ and, matrix $\mathbf{C_{UP}} = \mathbf{I}(3\times 3)$, $\mathbf{A_{UP(3\times 3)}} = (1 - \frac{RT_s}{L})\mathbf{I}_{(3\times 3)}$.

The general expression for the prediction model over N-step prediction horizon can be derived by using the approach discussed in Section II. For upper load control, the input sequence over predefined horizon can be defined in (31).

$$\mathbf{U_{UP}} = \begin{bmatrix} S_{AU}(k) & S_{AU}(k+1) & \dots & S_{AU}(k+N-1) \\ S_{BU}(k) & S_{AU}(k+1) & \dots & S_{AU}(k+N-1) \\ S_{CU}(k) & S_{AU}(k+1) & \dots & S_{AU}(k+N-1) \end{bmatrix}_{3\times N-1} = \left[\, \mathbf{u_{UP}}(k)\ \mathbf{u_{UP}}(k+1) \dots \mathbf{u_{UP}}(k+N-1) \,\right]_{3\times N-1} \quad (31)$$

The cost function for controlling the upper load is defined as

$$g_{UP} = \left|\mathbf{y^{*}_{UP}}(k+1) - \mathbf{y_{UP}}(k+1)\right| + \dots + \left|\mathbf{y^{*}_{UP}}(k+N) - \mathbf{y_{UP}}(k+N)\right| \quad (32)$$

In (32), the superscript "$*$" denotes the references. Basically, each load current error term at corresponding sampling instants are introduced in the cost function. Thus, an optimum control input sequence that minimizes the cost over N prediction step is determined.

B. APPLICATION OF GATE SIGNALS

The determined optimum control inputs are applied to the converter with an arrangement. The input sequences that can be applied over a given period contain information about optimum voltage vectors for both load stages. NSI has three zero voltage vectors that produce zero voltage at both output stages. Furthermore, it has six upper-active vectors and six lower-active vectors. The upper load voltage is nonzero whereas the lower load voltage is zero for the case in which one of the upper-active vectors is applied to the converter.

On the other hand, the lower load voltage is nonzero whereas the upper load voltage is zero for the case in which one of the lower-active voltage vectors is applied to the converter. The voltage vectors used in proposed control scheme is tabulated in Table 1 with the corresponding NSI switch positions. The exemplification of application of gate signals is presented in Fig. 6. From Fig. 6, the optimum voltage vector sequence of upper load is $\mathbf{V_{Uopt}} = [\mathbf{V_1}, \mathbf{V_2}, \mathbf{V_3}, \dots]$and the optimum voltage of lower load is $\mathbf{V_{Lopt}} = [\mathbf{V_3}, \mathbf{V_5}, \mathbf{V_2}, \dots]$ at sampling instant k. According to receding horizon strategy, the first elements of optimum input sequences are selected for the next time interval. Hence, $\mathbf{V_1}$ is selected as the control input for upper load control problem, and $\mathbf{V_3}$ is selected as the control input for lower load control problem. During the application of $\mathbf{V_1}$ to upper load stage, the lower

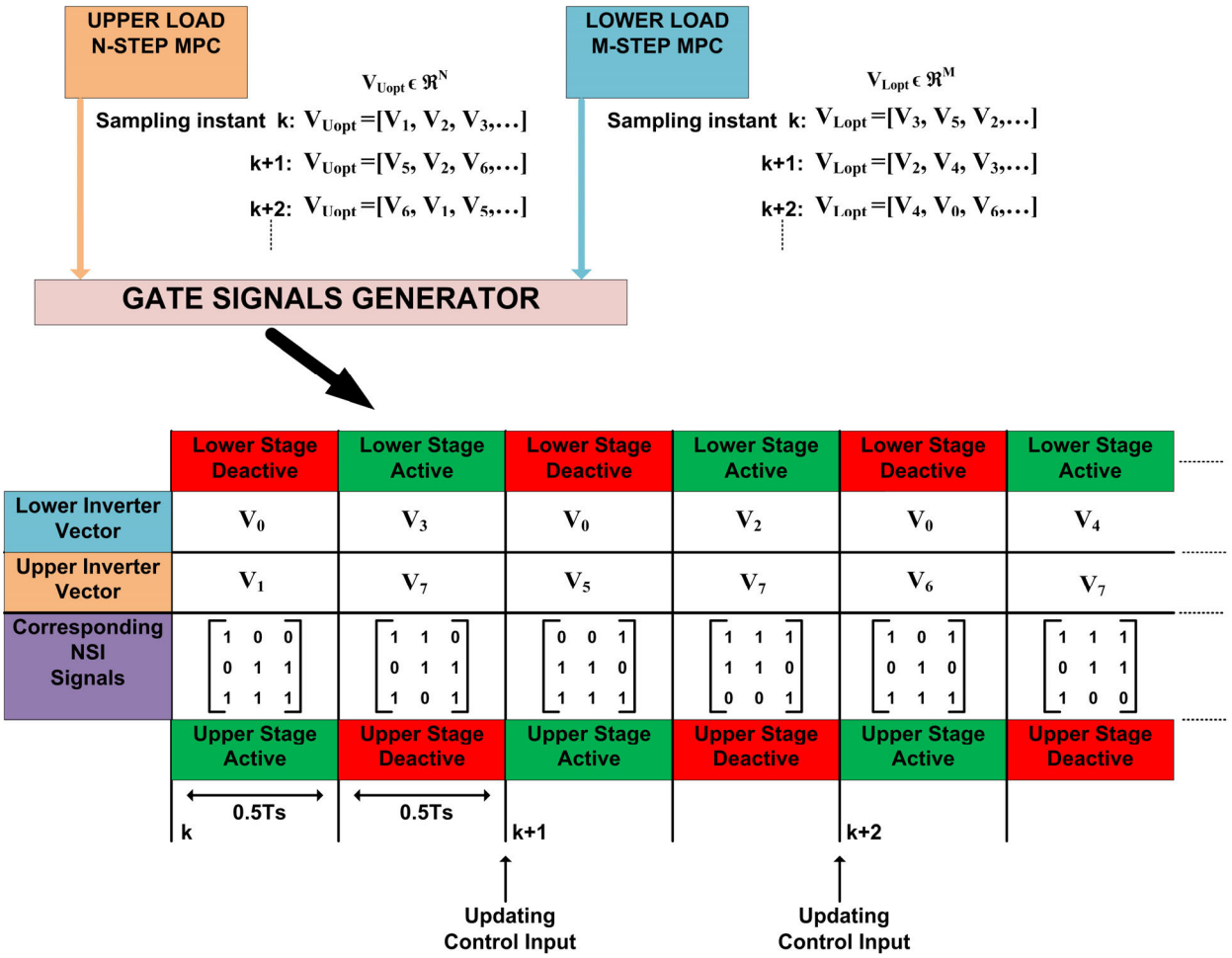

FIGURE 6. Exemplification of gate signals application. Optimum control inputs of upper load stage and lower load stage are sequentially applied to the NSI. Corresponding NSI signals = $[S_{AU}S_{BU}S_{CU}; S_{AM}S_{BM}S_{CM}; S_{AL}S_{BL}S_{CL}]$.

load stage is deactivated by applying the zero voltage vector $\mathbf{V_0}$. It is worth mentioning that to control the both load stages using unconnected MPC blocks yields 64 different possible solutions. Unfortunately, most of these 64 possible cannot be directly applied to NSI due to its switching restrictions. This is the main reason of why one of the load stages is deactivated when the other one is in active mode. Once the application of the optimum voltage vector to upper load stage is over, the optimum voltage vector $\mathbf{V_3}$ that minimizes the lower load current error is applied to the NSI. During this period which is called *Upper Stage Deactive,* a zero voltage vector $\mathbf{V_7}$ is applied to the upper load. Basically, each load stage is activated for a half period of sampling time and desired optimum vectors are applied to the load stages. The presented method of applying the voltage vectors to NSI is effortless and quite intuitive. The associated nine-switch inverter gate positions are selected according to optimum voltage vectors determined by unconnected MPC blocks. This process is repeated during each sampling interval and control inputs are updated depending on new measurements. For this system, it is desired that the load current errors of each load stages are minimum to ensure good dynamic performance. For that reason, the two optimum independent vectors that minimize the load current errors are synthesized by the presented gate signal generator.

C. OPTIMIZATION PROCESS OF MULTI-STEP DIRECT MODEL PREDICTIVE CONTROL

Model predictive control solves an optimal control problem over a receding horizon, subject to system constraints, to determine the next control action. The optimization is reinitialized and repeated at each subsequent time step. However, the optimization problem is difficult to solve except for problems with very short horizons. In this work, the exhaustive search is feasible only when prediction horizon is selected as 1 or 2. As prediction horizon is enlarged, the number of candidate solutions is increased. For the prediction horizon N = 3, nine-switch inverter has 3375 switching sequences when the conventional model predictive control is chosen as a control strategy. It is obvious that to perform an exhaustive search is clearly impractical. To overcome this problem, sub-finite sets are defined depending on control constraints and an optimum control sequence is determined. The main idea of the proposed optimization process is that decent input sequence

TABLE 1. Switching combinations of nine-switch inverter.

Upper VSI Vector	Lower VSI Vector	*Corresponding NSI Switch Position
**V_7	V_0	[1 1 1;1 1 1;0 0 0]
V_0	V_0	[0 0 0;1 1 1;1 1 1]
V_7	V_7	[1 1 1;1 1 1;0 0 0]
V_1	V_0	[1 0 0;0 1 1;1 1 1]
V_2	V_0	[1 1 0;1 1 1;0 0 1]
V_3	V_0	[0 1 0;1 0 1;1 1 1]
V_4	V_0	[0 1 1;1 0 0;1 1 1]
V_5	V_0	[0 0 1;1 1 0;1 1 1]
V_6	V_0	[1 0 1;0 1 0;1 1 1]
V_7	V_1	[1 1 1;1 0 0;0 1 1]
V_7	V_2	[1 1 1;1 1 0;0 0 1]
V_7	V_3	[1 1 1;0 1 0;1 0 1]
V_7	V_4	[1 1 1;0 1 1;1 0 0]
V_7	V_5	[1 1 1;0 0 1;1 1 0]
V_7	V_6	[1 1 1;1 0 1;0 1 0]

*NSI switch position = [S_{AU} S_{BU} S_{CU}; S_{AM} S_{BM} S_{CM}; S_{AL} S_{BL} S_{CL}]
**V_0 and V_7 are the zero vectors. Other vectors are the active vectors.

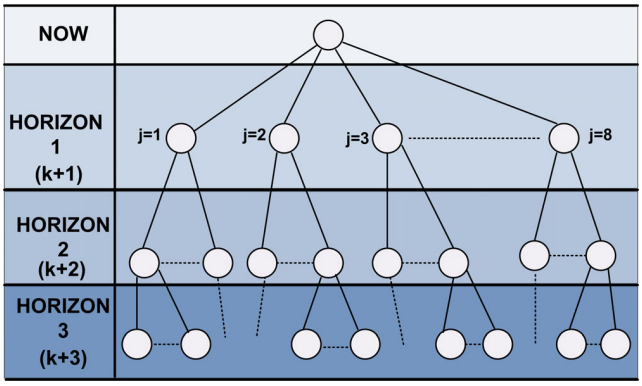

FIGURE 7. Visualization of the search tree for the prediction horizon N = 3. This search tree configuration is for proposed asymmetric multi-step MPC. Each load has its own search tree.

can determined by introducing specific dynamics or static constraints instead of searching the optimum point in whole big solution set. In proposed asymmetrical multi-step MPC, 512 possible control sequence are available for each load control problem for the prediction horizon N = 3. The search tree is shown in Fig. 7 for the case of N = 3. Instead of doing exhaustive search, most of the redundant solutions can be eliminated. To decrease the solution set, the condition defined in (33) can be used for budding the search tree. The switching states only that meet the criteria at prediction step (k+1) are used to calculate the objective error term at next sampling instant (k+2).

$$\left|i_o^*(k+N) - i_o(k+N)\right| \leq \Gamma(k+N) \tag{33}$$

where,

$$\Gamma(k+N) = i_o^*(k+N)\Upsilon \tag{34}$$

In (33) and (34), Γ is the maximum error tolerance for the load current. This control constraint is determined by using a load current reference vector and normalized current error parameter Υ. To obtain a good load current tracking capability, maximum error tolerance can be chosen as 2%

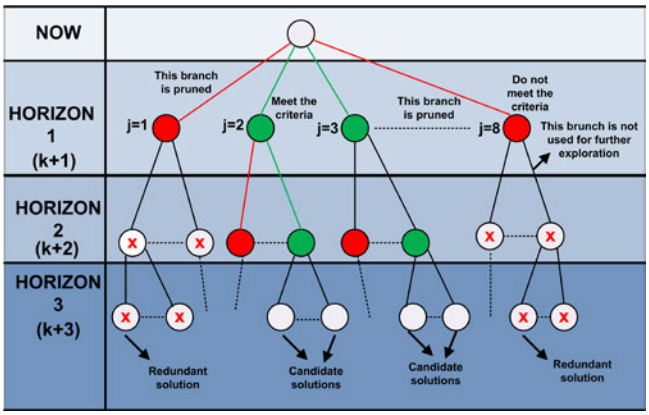

FIGURE 8. Example of tree diagram for the prediction horizon N = 3. The red nodes represent those that do not satisfy the criteria defined in (33). The green nodes represent those that satisfy the criteria defined in (33).

which corresponds to $\Upsilon = 0.02$. Note that the parameter Υ has a clear interpretation in terms of relative current error. The exploration of an optimum solution is exemplified in Fig. 8 for the prediction horizon N = 3.

In exemplification presented in Fig. 8, the node 2 and the node 3 meet the control constraint criteria defined in (33). These two nodes are selected for load current calculation at sampling instant (k+2). The other nodes at sampling instant (k+1), which are the red nodes, do not meet the criteria and they are removed from the solution set. Note that many redundant solutions are eliminated at sampling instant (k+1), (k+2) and (k+3) by just defining intuitive control constraint. The associated branches (the red ones) are pruned from the search tree and the nodes on these branches will be ignored. By using the same approach, all nodes meet the condition at each prediction step are identified. Then, an exhaustive search is performed to determine an optimum input sequence by using reduced sub-finite solution sets. The exemplification of solution set of asymmetrical multi-step MPC method is presented in Fig. 9. In Fig. 9, gray solutions represent those that were not explored by the searching algorithm. The green states are those that meet the relative error condition at an associated prediction step.

Fundamentally, the solutions that comply with the maximum relative current error criteria are open for exploration whereas a noncompliant solution serves as a dead end because it offers no improvement. Once a candidate solution is found, this solution is recorded as a temporary optimum control sequence of the system. The last complete solution that was discovered as a better optimum is declared the official optimum solution after the searching process is finished. In exemplification presented by Fig. 9, 16 nodes were visited to indentify the sub-solution sets. Then, 32 nodes are involved in the exhaustive search process. In brief, 48 nodes out of 512 nodes were visited to determine the constrained solution of the system. Conventionally, the costs associated with all possible 512 control inputs are evaluated to find the best control input. However, this is computationally expensive and it increases the system complexity. The computational

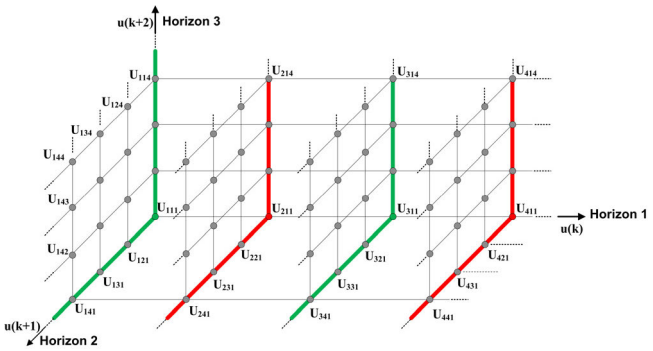

(a) Step 1: Determination of the solutions that meet the condition (33) on the horizon 1 axes (Prediction step 1). Only state 1 and state 3 satisfy the maximum load current error tolerance condition at sampling instant (k+1). They are selected as candidate solutions in the first prediction step.

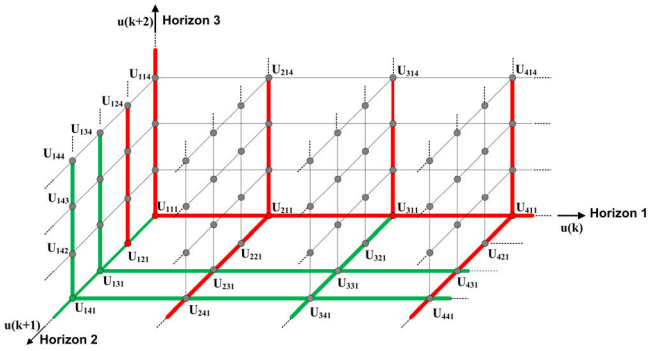

(b) Step 2: Determination of the solutions that meet the condition (33) on the horizon 2 axes (Prediction step 2). Only state 3 and state 4 satisfy the maximum load current error tolerance condition at sampling instant (k+3). They are selected as candidate solutions in the second prediction step.

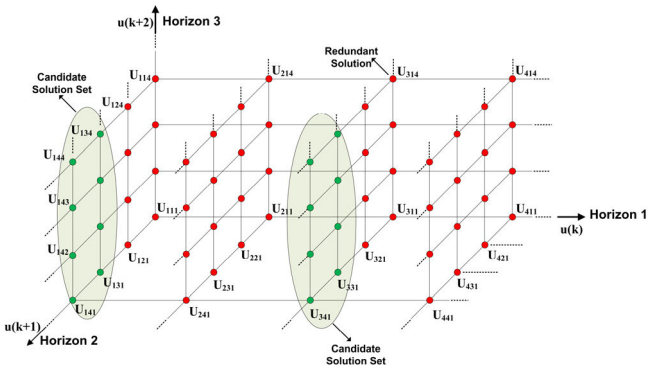

(c) Performing an exhaustive search in sub-finite solution sets to decide the best control sequence.

FIGURE 9. Exemplification of elimination process of redundant nodes from solution set.

complexity waveform is presented in Fig. 10 to show how competition burden increases as prediction horizon is enlarged. When the load current is calculated for more prediction steps, online computational complexity is significantly increases.

IV. EXPERIMENTAL RESULTS

A 3.2 kW nine-switch inverter prototype was built to verify the proposed asymmetrical multi-step model predictive

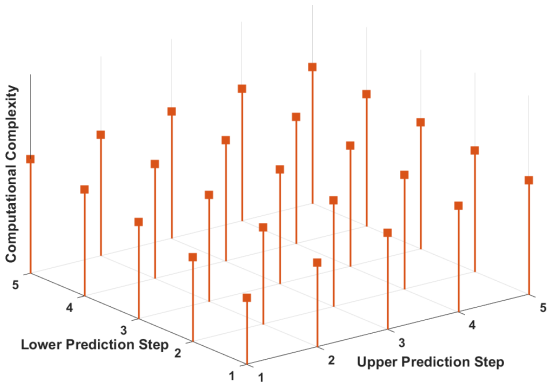

FIGURE 10. Computational complexity of proposed asymmetrical multi-step model predictive control method for different prediction steps.

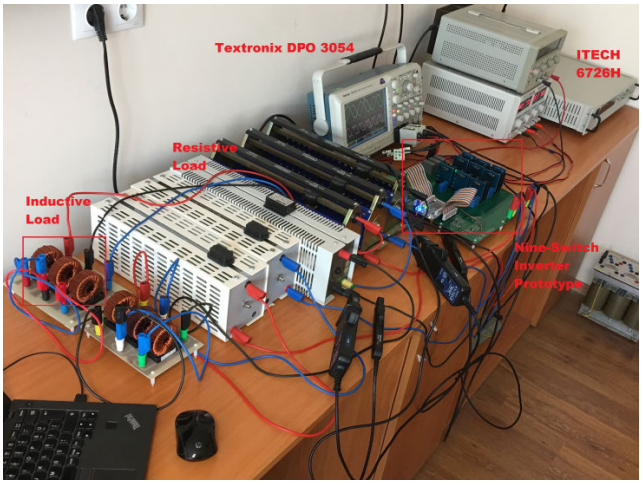

FIGURE 11. Experimental setup for nine-switch inverter systems as built in the laboratory.

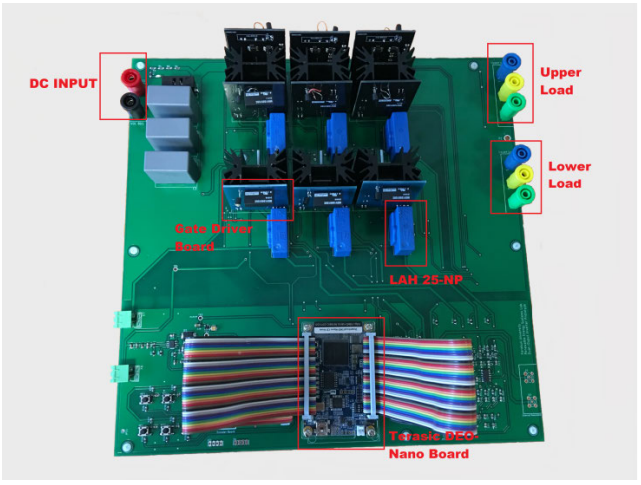

FIGURE 12. 3.2 kW nine-switch inverter proof-of-concept prototype employed to verify theoretical analysis.

control method. A picture of the physically constructed system is shown in Fig. 11 and two sets of RL loads are connected to the power stage. A close up picture of the nine-switch inverter prototype highlights the gate driver

TABLE 2. The key devices of the prototype.

Name	Company	Model
Power MOSFET	IXYS	IXTQ460P2
Current Transducer	LEM	LAH 25-NP
Voltage Transducer	LEM	LV-25P
A/D Converter	Texas Instruments	ADC128Sx
Controller Board	Terasic	DEO-Nano Cyclone IV
Gate Driver	Fairchild	FAN3122
Input Filter	KEMET	3x3.3uF

TABLE 3. Experimental parameters.

Parameters	Variables	Values
Dc-link Voltage	V_{dc}	60 V
Upper Load Resistance	R_{up}	3 Ω
Upper Load Inductance	L_{up}	3.5 mH
Lower Load Resistance	R_{low}	3 Ω
Lower Load Inductance	L_{low}	3.5 mH
Normalized Current Error	Υ	0.02
Sampling Time	Ts	20 µs
Input Capacitance	C_{in}	9.9 µF

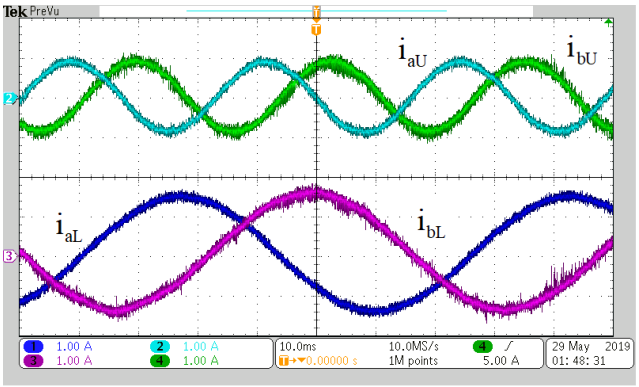

FIGURE 13. Steady-state performance of the proposed method. Channel 1 is i_{aL}, Channel 2 is i_{aU}, Channel 3 is i_{bL}, Channel 4 is i_{bU}. Upper load reference is 30 Hz/ 1 A. Lower load reference is 15 Hz/1.5 A (CASE A).

board, current transducer and FPGA board in Fig. 12. Discrete predictive control of the nine-switch inverter is accomplished using Altera Cyclone IV FPGA (Terasic DEO-Nano Board). The proposed control algorithm is realized in a pipelined architecture. The complex trigonometric and quadratic functions are calculated using a coordinate rotation digital computer (CORDIC) algorithm. The key devices of the prototype are tabulated in Table 2.

A. STEADY-STATE OPERATION

The performance of the proposed asymmetrical direct model predictive control is examined at steady-state operation for the various prediction steps. The experimental parameters of the proposed method are tabulated in Table 3. The following six cases are considered to evaluate the steady-state performance of the proposed approach:

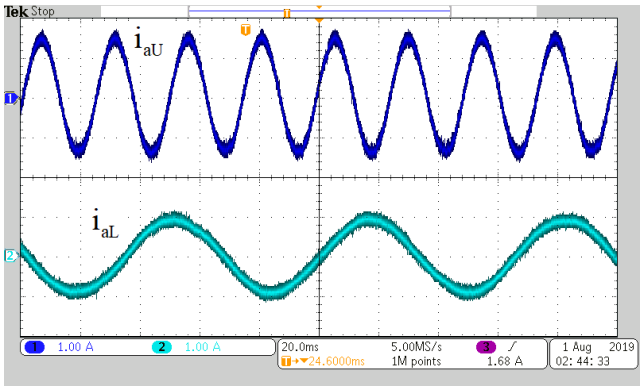

FIGURE 14. Steady-state performance of the proposed method. Channel 1 is i_{aU}, Channel 2 is i_{aL}. Upper load reference is 45 Hz/ 1.5 A. Lower load reference is 15 Hz/1 A (CASE A).

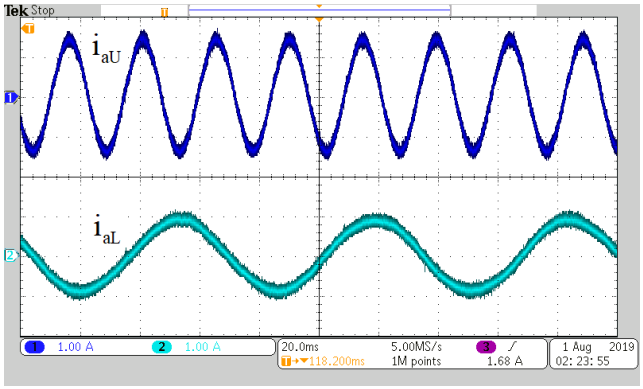

FIGURE 15. Steady-state performance of the proposed method. Channel 1 is i_{aU}, Channel 2 is i_{aL}. Upper load reference is 45 Hz/ 1.5 A. Lower load reference is 15 Hz/1 A (CASE B).

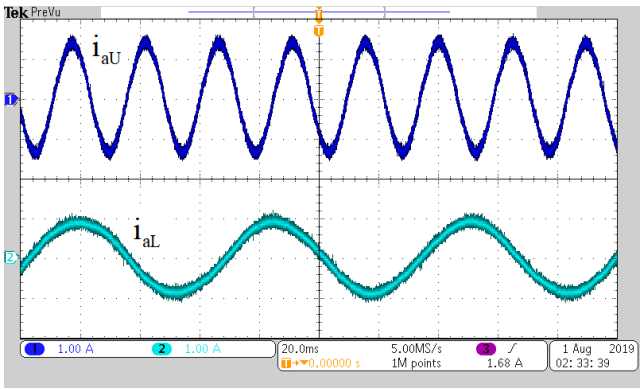

FIGURE 16. Steady-state performance of the proposed method. Channel 1 is i_{aU}, Channel 2 is i_{aL}. Upper load reference is 45 Hz/ 1.5 A. Lower load reference is 15 Hz/1 A (CASE C).

- Case A: upper load prediction step N = 1 and lower load prediction step M = 1.
- Case B: upper load prediction step N = 2 and lower load prediction step M = 1.
- Case C: upper load prediction step N = 3 and lower load prediction step M = 1.
- Case D: upper load prediction step N = 1 and lower load prediction step M = 2.

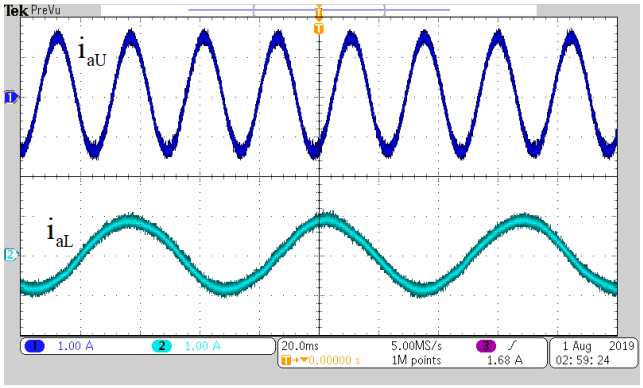

(a) Experimental results for Case D in steady-state

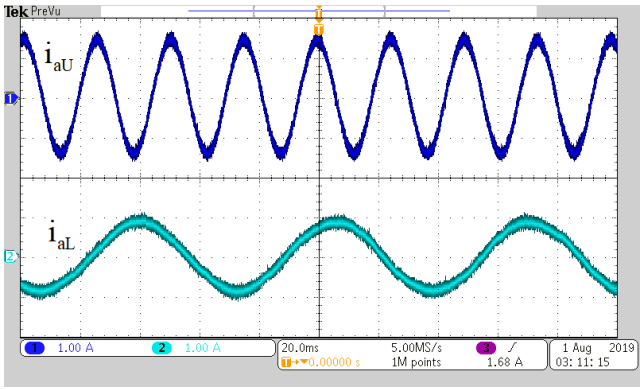

(b) Experimental results for Case E in steady-state

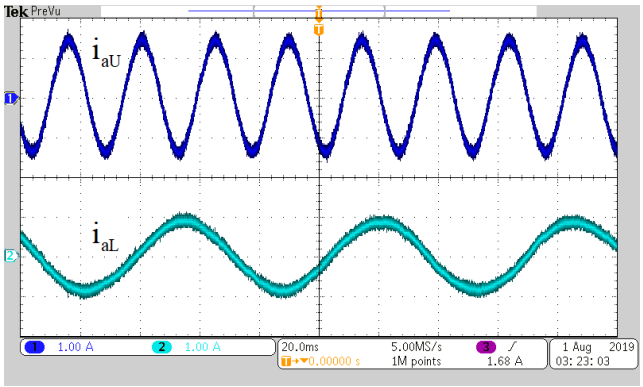

(c) Experimental results for Case F in steady-state.

FIGURE 17. Steady-state performance of the proposed method. Channel 1 is i_{aU}, Channel 2 is i_{aL}. Upper load reference is 45 Hz/ 1.5 A. Lower load reference is 15 Hz/1 A. (a) Steady-state performance of the proposed method (Case D). (b) Steady-state performance of the proposed method (Case E). Steady-state performance of the proposed method (Case F).

- Case E: upper load prediction step N = 2 and lower load prediction step M = 2.
- Case F: upper load prediction step N = 3 and lower load prediction step M = 2.

The experimental results for Case A are presented in Figs. 13-14. The references with different peak and frequency are introduced to upper load stage and lower load stage. In Fig. 13, output load currents are presented when the upper load current reference is 30 Hz/1 A and the lower load current reference 15 Hz/1.5 A. According to experimental

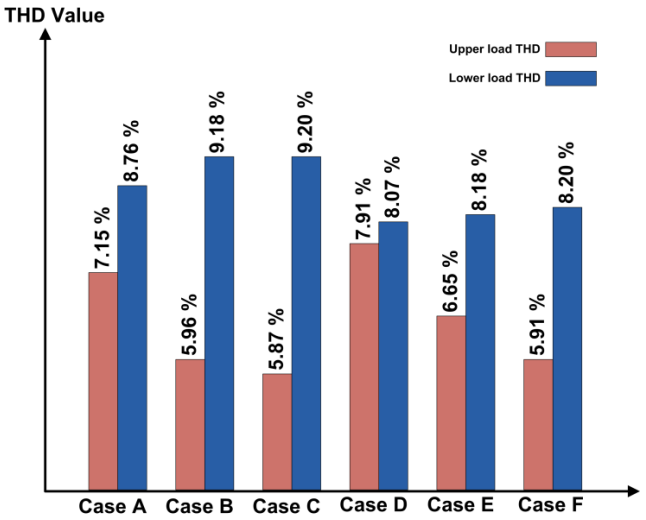

FIGURE 18. THD values of upper load and lower load for different cases.

results, NSI combined with the proposed method provides good steady-state operation. In order to test asymmetrical multi-step MPC, different prediction steps are selected for upper load control and lower load control. Fig. 15 and Fig. 16 present the steady-state experimental results for Case B and Case C, respectively. In Case A, Case B and Case C, the noticeable point is that the upper load current Total Harmonic Distortions (THD) decreases as the prediction step of upper load increases. The upper load THD is 7.15% for Case A, 5.96% for Case B and 5.87% for Case C.

The experimental results for Case D, Case E and Case F are presented in Fig. 17. According to steady-state experimental waveforms, the proposed method provides a robust and reliable operation. Each load current is separately regulated to match with its utilization profile within specific workload. Both load stages are independently controlled with using different prediction steps.

The key criterion related to the control performance is the current THD. The detailed THD analysis of the two load currents under different operating conditions was performed and it is reported in Fig. 18. Horizons longer than one reduce the close-loop costs of both unconnected MPC problems when compared to the one with single prediction horizon. However, minor reductions in upper load current and lower load current THD are achieved. The load currents THD can be further reduced by increasing prediction steps. But this also increases the computational complexity of the online optimization process. In conclusion, load current quality is improved as the prediction horizon is increased and the proposed control method achieves a good load current tracking performance in steady-state.

B. PERFORMANCE DURING TRANSIENTS

In order to evaluate performance of the proposed direct model predictive control approach during transient, several system steps are applied to the system. The Fig. 19 shows the

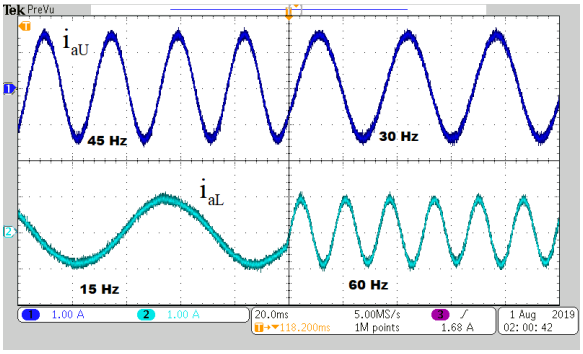

(a) The dynamic performance of the proposed method (CASE A).

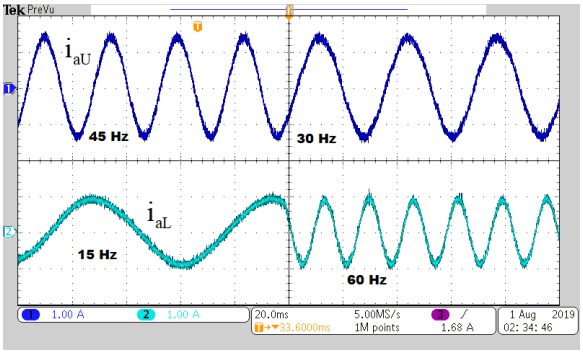

(b) The dynamic performance of the proposed method (CASE C).

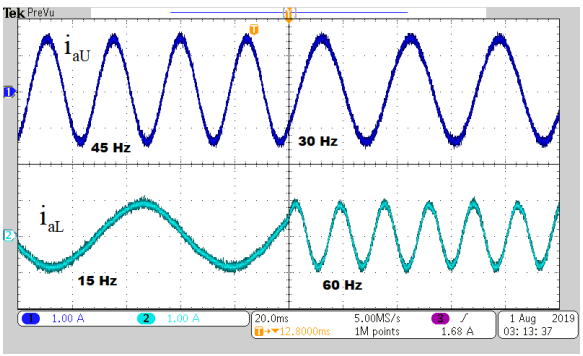

(c) The dynamic performance of the proposed method (CASE E).

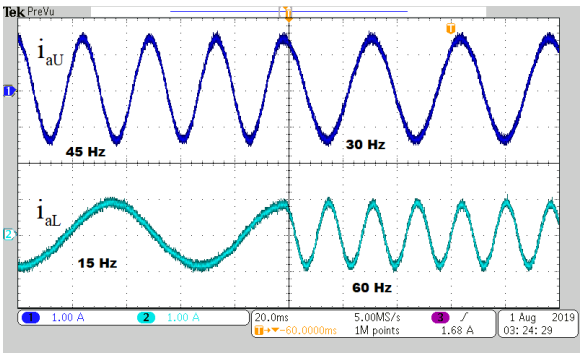

(d) The dynamic performance of the proposed method (CASE F).

FIGURE 19. Transient performance of the proposed method. Channel 1 is i_{aU}, Channel 2 is i_{aL}. The upper load step is from 45 Hz/ 1.5 A to 30 Hz/ 1.5 A. The lower load step is from 15 Hz/1 A to 60 Hz/1 A.

dynamic response of the proposed method under the different conditions. For all cases, the upper load system step is from

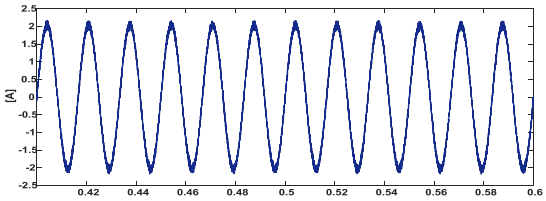

(a) Upper load current waveform. The reference is 2 A/ 60 Hz.

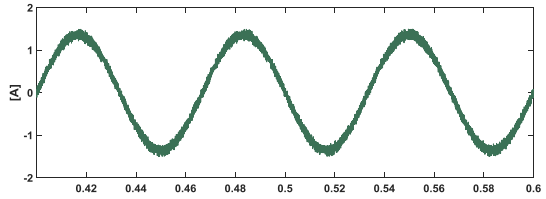

(b) Lower load current waveform. The reference is 1.5 A/ 15 Hz.

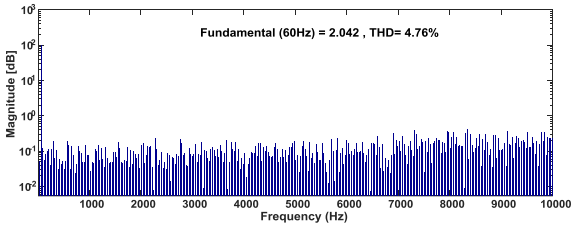

(c) Frequency spectrum of upper load current.

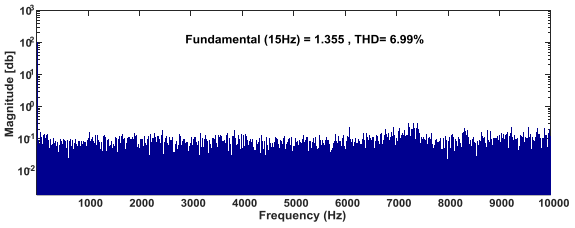

(d) Frequency spectrum of lower load current.

FIGURE 20. The experimental waveforms and FFT analysis of load currents at both stages when the proposed method is applied to the system.

45 Hz/ 1.5 A to 30 Hz/1.5 A, and the lower load system step is from 15 Hz/ 1 A to 60 Hz/1 A. During frequency transitions, the proposed technique was able to track new set points and there was no any unwanted interaction between upper load stage and lower load stage. From the experimental results presented in Fig. 19, both ac loads are safely controlled by using the proposed control approach without overshoot or cross coupling current. The two different system steps were applied to the NSI and the unconnected MPC controllers successfully compensated the load current errors. The proposed method achieves an excellent dynamic performance and it is capable of provide a reliable converter operation. The point that needs to be highlighted is that the horizon length does not have significant impact on transient performance. The increase in the prediction step did not provide a faster dynamic response. This means that the control bandwidth approximately stays the same despite increasing the prediction horizon. It is concluded that the dynamic performance of the proposed predictive control is effectively limited to the available voltage vectors regardless of the length of the prediction horizon.

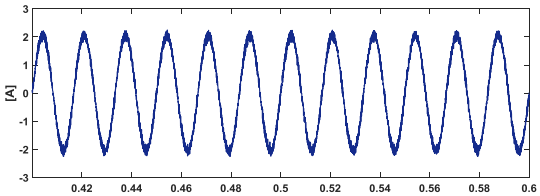

(a) Upper load current waveform. The reference is 2 A/ 60 Hz.

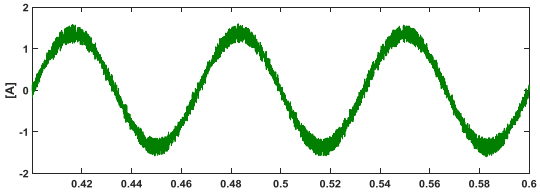

(b) Lower load current waveform. The reference is 1.5 A/ 15 Hz.

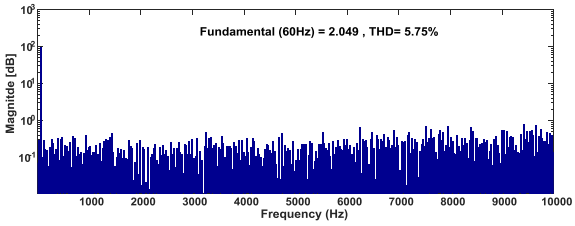

(c) Frequency spectrum of upper load current.

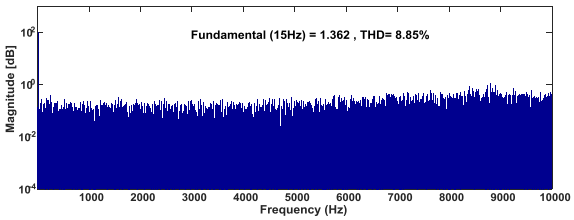

(d) Frequency spectrum of lower load current.

FIGURE 21. The experimental waveforms and FFT analysis of load currents at both stages when the conventional MPC method is applied to the system.

C. CONVENTIONAL MPC vs PROPOSED METHOD

In this section, the comparison results between conventional MPC scheme (see Fig. 4) and the proposed MPC scheme (see Fig. 5) are presented for the case in which the upper load prediction horizon and the lower load prediction horizon are selected as 2. The comparisons are made in terms of load current THD and the transient performances. The data captured by the scope (Tektronix DPO 3054) have been imported into MATLAB to carry out Fast Fourier Transform (FFT) analysis. Fig. 20 presents the experimental results for the proposed method and Fig. 21 presents experimental results for the conventional method. FFT analysis was carried out up to 10 kHz to calculate the spectral contents.

According to FFT results, the upper load current THD is 4.76% and the lower load THD is 6.99% when the proposed method is applied to the system. On the other hand, the upper load THD is 5.75% and the lower load THD is 8.85% when the conventional MPC is applied to the system. It can be easily deduced that the proposed method provides minor reduction in load current THD compared to the one with the

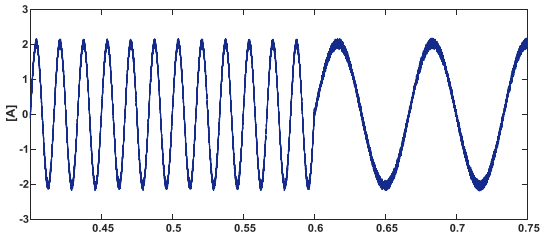

(a) Dynamic response of the proposed method (Upper Load).

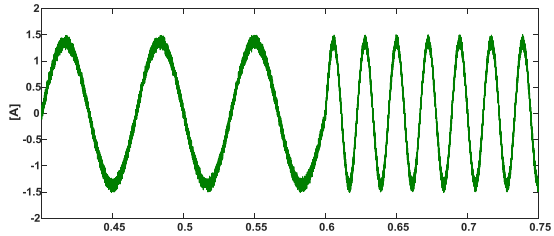

(b) Dynamic response of the proposed method (Lower Load)

FIGURE 22. Transient performance of the proposed method. The upper load step is from 60 Hz/ 2 A to 15 Hz/ 2 A. The lower load step is from 15 Hz/1.5 A to 45 Hz/1.5 A.

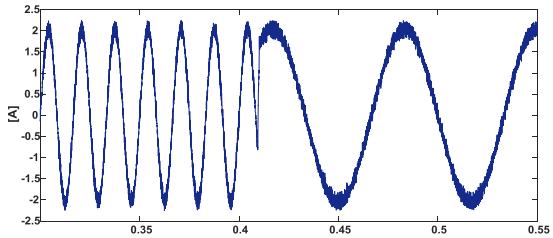

(a) Dynamic response of the proposed method (Upper Load).

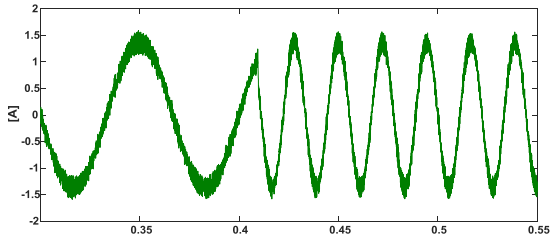

(b) Dynamic response of the proposed method (Lower Load).

FIGURE 23. Transient performance of the conventional MPC method. The upper load step is from 60 Hz/ 2 A to 15 Hz/ 2 A. The lower load step is from 15 Hz/1.5 A to 45 Hz/1.5 A.

conventional MPC method. The THD is mostly caused by the first few harmonics and there is no any significant difference between the proposed method and the conventional MPC in terms of load current quality. In order to make a comparison in terms of transient performance, identical system step is applied to the both systems.

Fig. 22 and Fig. 23 show the dynamic response of the proposed method and the conventional MPC, respectively. Good tracking of the references is observed. The upper load system step and the lower load system step are applied to at same time. According to results presented in Fig. 22 and Fig. 23, both control methods provide fast response to load variations and maintain control of each load current independently.

V. CONCLUSION

This paper proposes a novel asymmetrical multi-step model predictive control of nine-switch inverter. The proposed method provides a flexibility to choose independent prediction horizon for controlling the individual loads. Two unconnected MPC problems are formulated and each load is assumed to be controlled by a virtual voltage source inverter. The determined optimum switching combinations are sequentially applied to the nine-switch inverter and two separate loads are controlled without any undesirable interactions. Thanks to the proposed method, complete independent control of two ac loads is achieved when multi step model predictive control is applied to the system.

REFERENCES

[1] C. Liu, B. Wu, N. R. Zargari, D. Xu, and J. Wang, "A novel three-phase three-leg AC/AC converter using nine IGBTs," *IEEE Trans. Power Electron.*, vol. 24, no. 5, pp. 1151–1160, May 2009.

[2] C. Liu, B. Wu, N. Zargari, and D. Xu, "A novel nine-switch PWM rectifier-inverter topology for three-phase UPS applications," in *Proc. Eur. Conf. Power Electron. Appl.*, Aalborg, Denmark, 2007, pp. 1–10.

[3] L. Zhang, P. C. Loh, and F. Gao, "An integrated nine-switch power conditioner for power quality enhancement and voltage sag mitigation," *IEEE Trans. Power Electron.*, vol. 27, no. 3, pp. 1177–1190, Mar. 2012.

[4] M. Azizi, A. Fatemi, M. Mohamadian, and A. Y. Varjani, "Integrated solution for microgrid power quality assurance," *IEEE Trans. Energy Convers.*, vol. 27, no. 4, pp. 992–1001, Dec. 2012.

[5] S. M. Dehghan, M. Mohamadian, and A. Yazdian, "Hybrid electric vehicle based on bidirectional Z-source nine-switch inverter," *IEEE Trans. Veh. Technol.*, vol. 59, no. 6, pp. 2641–2653, Jun. 2010.

[6] S. Sharma, M. Aware, and A. Bhowate, "Direct torque control of symmetrical six-phase induction machine using nine switch inverter," in *Proc. IEEE Transp. Electrific. Conf. (ITEC-India)*, Pune, India, Dec. 2017, pp. 1–6.

[7] H. Zheng, T. Zou, J. Hu, and H. Yu, "A framework for adaptive predictive control system based on zone control," *IEEE Access*, vol. 6, pp. 49513–49522, 2018.

[8] W. Wang, Y. Li, J. Shi, and C. Lin, "Vibration control method for an electric city bus driven by a dual motor coaxial series drive system based on model predictive control," *IEEE Access*, vol. 6, pp. 41188–41200, 2018.

[9] G. Zhao and S. Yang, "Self-triggered model predictive control for linear systems with switched cost functions," *IEEE Access*, vol. 7, pp. 67726–67733, 2019.

[10] T. I. Bø, E. Vaktskjold, E. Pedersen, and O. Mo, "Model predictive control of marine power plants with gas engines and battery," *IEEE Access*, vol. 7, pp. 15706–15721, 2019.

[11] S. Vazquez, J. Rodriguez, M. Rivera, L. G. Franquelo, and M. Norambuena, "Model predictive control for power converters and drives: Advances and trends," *IEEE Trans. Ind. Electron.*, vol. 64, no. 2, pp. 935–947, Feb. 2017.

[12] F. Wang, X. Mei, J. Rodriguez, and R. Kennel, "Model predictive control for electrical drive systems-an overview," *CES Trans. Elect. Mach. Syst.*, vol. 1, no. 3, pp. 219–230, Sep. 2017.

[13] J. Scoltock, T. Geyer, and U. K. Madawala, "A model predictive direct current control strategy with predictive references for MV grid-connected converters with LCL-filters," *IEEE Trans. Ind. Electron.*, vol. 30, no. 10, pp. 5926–5937, Oct. 2015.

[14] R. O. Ramírez, J. R. Espinoza, C. R. Baier, M. Rivera, F. Villarroel, J. I. Guzman, and P. E. Melin, "Finite-state model predictive control with integral action applied to a single-phase Z-source inverter," *IEEE J. Emerg. Sel. Topics Power Electron.*, vol. 7, no. 1, pp. 228–239, Mar. 2019.

[15] T. Dragičević, "Dynamic stabilization of DC microgrids with predictive control of point-of-load converters," *IEEE Trans. Power Electron.*, vol. 33, no. 12, pp. 10872–10884, Dec. 2018.

[16] B. Gutierrez and S.-S. Kwak, "Modular multilevel converters (MMCs) controlled by model predictive control with reduced calculation burden," *IEEE Trans. Power Electron.*, vol. 33, no. 11, pp. 9176–9187, Nov. 2018.

[17] T. J. Vyncke, S. Thielemans, and J. A. Melkebeek, "Finite-set model-based predictive control for flying-capacitor converters: Cost function design and efficient FPGA implementation," *IEEE Trans. Ind. Informat.*, vol. 9, no. 2, pp. 1113–1121, May 2013.

[18] Y. Zhang and W. Xie, "Low complexity model predictive control—Single vector-based approach," *IEEE Trans. Power Electron.*, vol. 29, no. 10, pp. 5532–5541, Oct. 2014.

[19] F. Salinas, M. A. González, and M. F. Escalante, "Finite control set-model predictive control of a flying capacitor multilevel chopper using Petri nets," *IEEE Trans. Ind. Electron.*, vol. 63, no. 9, pp. 5891–5899, Sep. 2016.

[20] S. Kwak, S.-J. Yoo, and J. Park, "Finite control set predictive control based on Lyapunov function for three-phase voltage source inverters," *IET Power Electron.*, vol. 7, no. 11, pp. 2726–2732, Nov. 2014.

[21] M. P. Akter, S. Mekhilef, N. M. L. Tan, and H. Akagi, "Modified model predictive control of a bidirectional AC–DC converter based on Lyapunov function for energy storage systems," *IEEE Trans. Ind. Electron.*, vol. 63, no. 2, pp. 704–715, Feb. 2016.

[22] M. Easley, S. Jain, M. B. Shadmand, and H. Abu-Rub, "Computationally efficient distributed predictive controller for cascaded multilevel impedance source inverter with LVRT capability," *IEEE Access*, vol. 7, pp. 35731–35742, 2019.

[23] R. P. Aguilera and D. E. Quevedo, "Predictive control of power converters: Designs with guaranteed performance," *IEEE Trans Ind. Informat.*, vol. 11, no. 1, pp. 53–63, Feb. 2015.

OZAN GULBUDAK (S'14–M'16) received the B.Sc. and M.Sc. degrees in electrical engineering from Mersin University, Turkey, in 2008 and 2010, respectively, and the Ph.D. degree from the University of South Carolina, Columbia, USA. Since 2017, he has been with Karabuk University, where he is currently an Assistant Professor. His research interests include model predictive control, development of control platforms based on FPGA, direct matrix converters, inverter topologies, and motor drives.

MUSTAFA GOKDAG received the B.S. degree (Hons.) in electrical and electronics engineering from Firat University, Turkey, in 2009, and the M.Sc. and Ph.D. degrees in electrical and electronics engineering from Karabuk University, Turkey, in 2011 and 2016, respectively. From 2009 to 2016, he was a Research Assistant with the Department of Electrical and Electronics Engineering, Karabuk University, where he has been an Assistant Professor, since 2016. His research interests include modeling and control of dc-dc power converters and model predictive control of ac-dc, dc-ac, and ac-ac power converters for renewable and electrical drives.